The Innovation, Volume *3*

Supplemental Information

Multifunctional succinate additive for flexible perovskite solar cells with more than 23% power-conversion efficiency

Minghao Li, Junjie Zhou, Liguo Tan, Hang Li, Yue Liu, Chaofan Jiang, Yiran Ye, Liming Ding, Wolfgang Tress, and Chenyi Yi

Supporting Information

Multifunctional succinate additive for flexible perovskite solar cells with more than 23% power conversion efficiency

Minghao Li[1], Junjie Zhou[1], Liguo Tan[1], Hang Li[1], Yue Liu[1], Chaofan Jiang[1], Yiran Ye[1], Liming Ding[2], Wolfgang Tress[3], Chenyi Yi[1,*]

[1] State Key Laboratory of Power System, Department of Electrical Engineering, Tsinghua University, Beijing, 100084, China.

[2] Center for Excellence in Nanoscience (CAS), Key Laboratory of Nanosystem and Hierarchical Fabrication (CAS), National Center for Nanoscience and Technology, Beijing 100190, China.

[3] Institute of Computational Physics (ICP) ZHAW School of Engineering Wildbachstr. 21, Winterthur 8400, Switzerland.

[*]Correspondence: yicy@tsinghua.edu.cn

Methods

Chemicals

The chemicals were purchased from commercial sources and used without further purification. MS was synthesized by first dissolving succinic acid in ethanol with vigorous stirring. Then, an excess of methylamine ethanol solution was added dropwise to the succinic acid solution and stirred for 2~3 hours. White participation appeared after stirring for a long time. The acquired powder was washed with diethyl ether several times to obtain pure MS.

Device Fabrication

FTO/glass substrates and PEN/ITO substrates were used for device fabrication and were first etched by laser and chemical etching (Zn/HCl), respectively. The flexible substrates were further attached onto FTO/glass substrates for mechanical support with PDMS.[1] All substrates were ultrasonically washed with detergent, deionized water, ethanol and isopropanol sequentially and then treated with UV-ozone for 20 min before electron transporting layer deposition. For FTO/glass substrates, a SnO_2 layer was deposited by chemical bath deposition as previously reported.[2] For flexible substrates, the conventional method was adopted by spin-coating the commercial SnO_2 nanoparticles (diluted 1:3) onto the substrates, followed by an annealing process at 150 ^oC for 30 min in ambient air. The process of perovskite thin film deposition, surface treatment and hole transporting layer deposition were all the same as we have reported previously.[3] In brief, after UV-ozone treatment, 1.5 M PbI_2 solution with 1~2 mol% CsI in DMF and DMSO (volume ratio 9:1) was first spun onto the SnO_2 layer at 1500 rpm. After annealing at 70 ^oC, organic ammonium salt (FAI: MAI: MACl = 90 mg: 6 mg: 9 mg) in IPA solution was then spun onto the PbI_2 layer at 2000 rpm. The obtained films were annealed at 150 ^oC for 15 min in an ambient environment. For the modified sample, MS were added to the PbI_2 precursor to obtain designated concentrations of MS-incorporated perovskite thin films. For the posttreatment process, the cooled perovskite films were treated with 10 mM 2-Br-PEAI/IPA solution at 4000 rpm and annealed at 100 ^oC for 10 min. For the hole transporting layer, spiro-OMeTAD solution was deposited at 4000 rpm for 20 s. Finally, back contact was deposited by thermally evaporating 80 nm Au. Anti-reflection film was deposited on the glass side of the device before measurement.

Characterization

The SEM images of the perovskite film were obtained on a Zeiss Merlin. An Agilent Cary 5000 UV-vis spectrophotometer was used to record the absorption spectra of the perovskite film. Photoluminescence and time-resolved PL decay results were collected on an Edinburgh FLSP920 system with an excitation source of 405 nm wavelength. Conventional XRD measurements of perovskite thin films were conducted on a Rigaku SmartLab (copper Kα, λ = 1.54 Å, 150 mA, 40 kV). GIXRD measurements were conducted using a Bruker D8 Advance (copper Kα, λ = 1.54 Å, 150 mA, 40 kV). A JEOL ECS-400 was utilized to collect the ^1H and ^{13}C NMR spectra of the samples in DMSO-d6.

Sun *J-V* measurements of the solar cells were performed under a Newport AAA solar simulator with a Keithley 2400 source meter. The light intensity was calibrated by an NREL certified silicon diode. An aperture area of 0.1 cm^2 or

1.0 cm^2 was achieved by using a dark metal mask with the designated area. The measurement was conducted in ambient air using unencapsulated devices. The stable output power of the devices was characterized by holding the device at a premeasured maximum power point bias voltage determined by the *J-V* measurement. The long-term stability of the devices (in N_2) under illumination was characterized with homemade multichannel MPPT instruments using an LED as the light source. The bending durability of the FPSCs was tested by homemade bending equipment with the corresponding bending radius, and the PCE was recorded after bending specific cycles.

DFT Calculations

The Vienna *Ab initio* Simulation Package (VASP) was employed to perform the first-principles calculations.[4] The Kohn-Sham equation was solved by using the plane wave basis set. The GGA-PBE exchange-correlation functional was selected to describe the electron interactions.[5] Valence-core interactions were described by projector-augmented-wave (PAW) pseudopotentials.[6] Grimme's DFT-D3 method was used for the van der Waals interaction correction.[7] The cutoff energy for the plane wave basis sets was 400 eV. Only the Γ-point was considered for calculations. All the optimizations were conducted until the residual of energy and forces decreased than $10^{-5}\ eV$ and $0.05\ eV/\text{Å}$, respectively. Two different perovskite surface situations (FAI-terminated and PbI_2 terminated) were modeled to evaluate the absorption energy of the succinate anions on the surfaces. The absorption energy is described by

$$E_{abs} = E_{MS+FAPbI_3} - E_{MS} - E_{FAPbI_3}$$

where E_{abs} is the absorption energy of the succinate anion, $E_{MS+FAPbI_3}$ is the energy of the whole system, and E_{MS} and E_{FAPbI_3} are the energies of the succinate anion and $FAPbI_3$ perovskite, respectively.

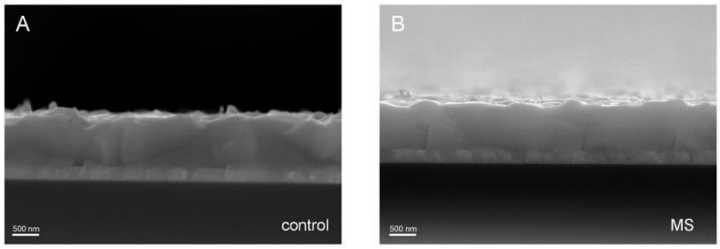

Figure S1. Cross-sectional SEM images of (A) Control, (B) MS-perovskite film.

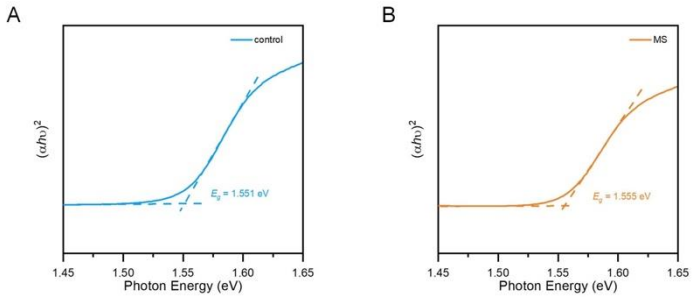

Figure S2. Tauc plot and acquired bandgap of the perovskite films from UV-vis characterization.

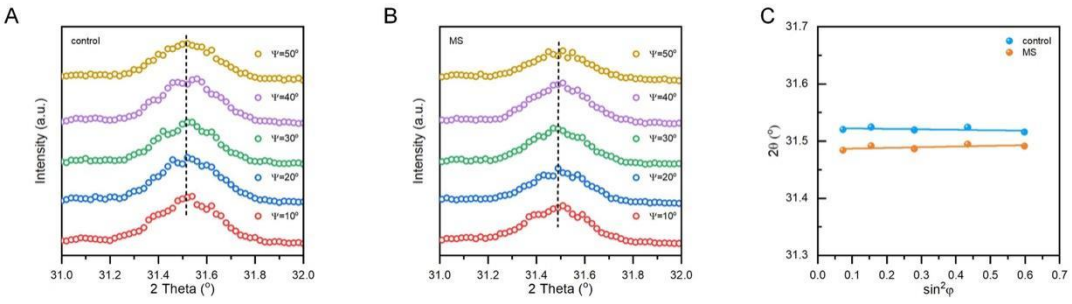

Figure S3. Residual strain analysis of the control and MS-perovskite on rigid FTO glass substrates. (A, B) GIXRD spectrum at different tilt angles for the (A) control and (B) MS perovskite. (C) Residual strain of the corresponding perovskite films.

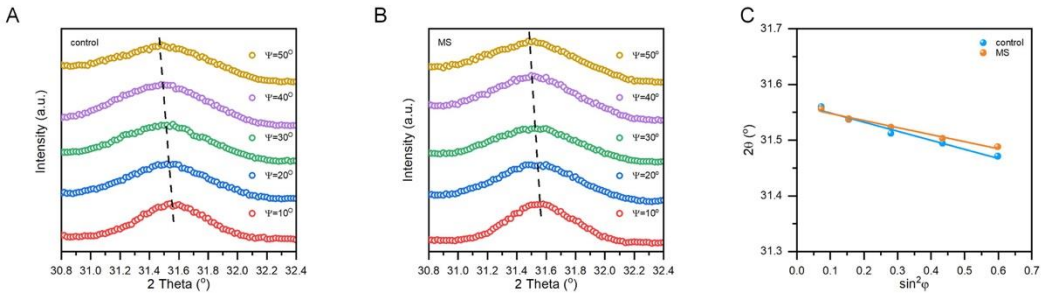

Figure S4. Residual strain analysis of the control and MS-perovskite on flexible substrates. (A, B) GIXRD spectrum at different tilt angles for the (A) control and (B) MS-perovskite. (C) Residual strain of the corresponding perovskite films.

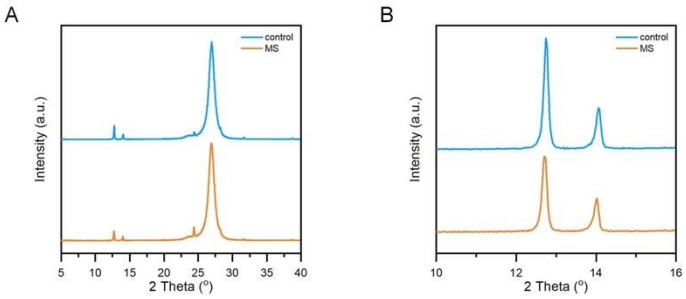

Figure S5. XRD spectra of the control and MS-perovskite thin films on PEN/ITO.

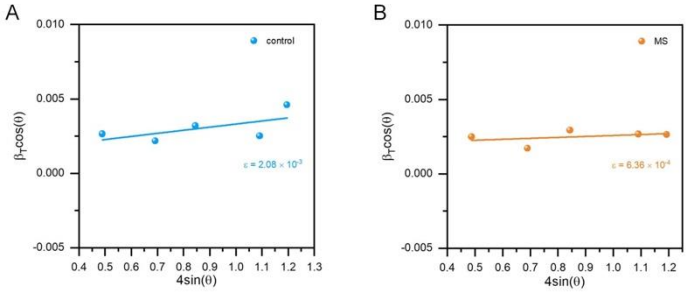

Figure S6. Microstrains in control and MS-perovskite on PEN/ITO substrates.

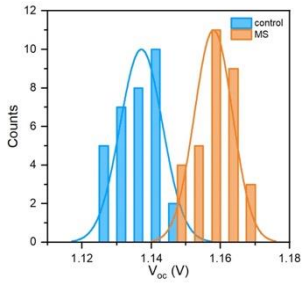

Figure S7. Open-circuit voltage (V_{oc}) distribution of the PSCs in the same batch.

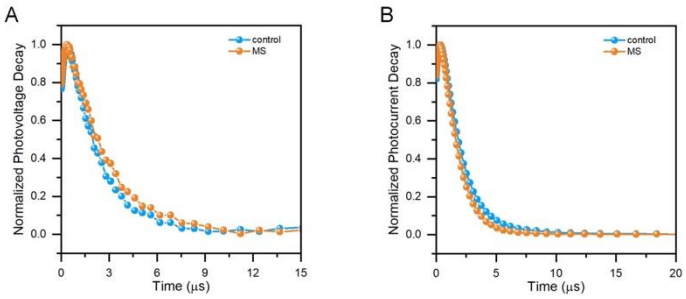

Figure S8. Normalized transient photovoltage and photocurrent decay of the control and MS-PSCs. The MS device demonstrates relatively slower photovoltage decay and faster photocurrent decay, in agreement with the increased V_{oc} and charge transport.

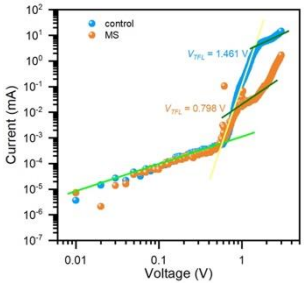

Figure S9. Space charge limited current (SCLC) measurements of the control and MS-perovskite incorporated electron only devices. Device structure: FTO/SnO_2/perovskite/PCBM/Au. The MS device shows a lower trap filling voltage. This trend supports that bulk defects are reduced due to MS incorporation.

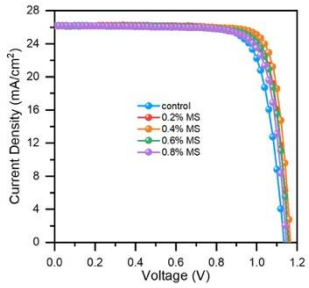

Figure S10. Typical *J-V* curves of rigid devices with different additive concentrations.

Table S1. Summary of the rigid device performance of the different MS concentrations.

MS concentration (%)	J_{sc} (mA/cm²)	V_{oc} (V)	FF (%)	PCE (%)
0	26.19	1.134	77.86	23.13
0.2	26.18	1.158	80.39	24.37
0.4	26.14	1.167	82.57	25.18
0.6	26.12	1.155	79.99	24.13
0.8	26.12	1.145	78.90	23.62

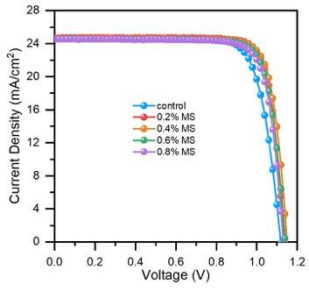

Figure S11. Typical J-V curves of flexible devices with different additive concentrations.

Table S2. Summary of the flexible device performance of the different MS concentrations.

MS concentration (%)	J_{sc} (mA/cm^2)	V_{oc} (V)	FF (%)	PCE (%)
0	24.69	1.119	78.02	21.56
0.2	24.64	1.146	79.99	22.59
0.4	24.60	1.149	81.93	23.17
0.6	24.56	1.141	81.14	22.74
0.8	24.53	1.131	80.52	22.34

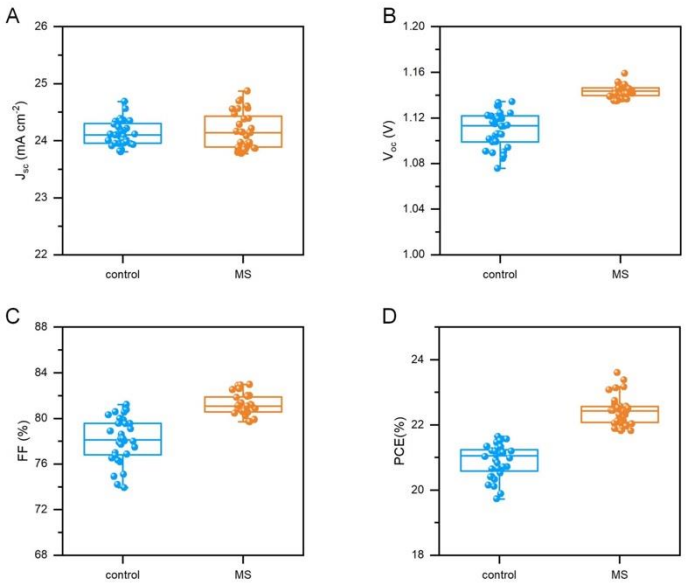

Figure S12. Statistical distribution of the photovoltaic metrics of the control and MS-FPSCs. (A) J_{sc}, (B) V_{oc}, (C) FF and (D) PCE.

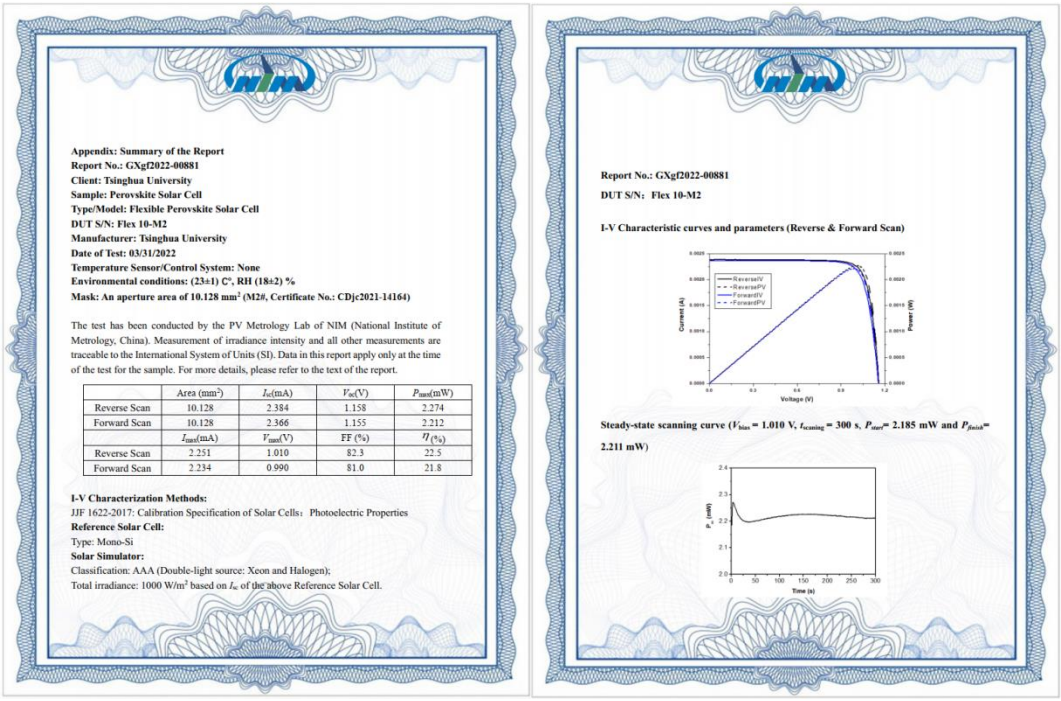

Appendix: Summary of the Report
Report No.: GXgf2022-00881
Client: Tsinghua University
Sample: Perovskite Solar Cell
Type/Model: Flexible Perovskite Solar Cell
DUT S/N: Flex 10-M2
Manufacturer: Tsinghua University
Date of Test: 03/31/2022
Temperature Sensor/Control System: None
Environmental conditions: (23±1) C°, RH (18±2) %
Mask: An aperture area of 10.128 mm² (M2#, Certificate No.: CDjc2021-14164)

The test has been conducted by the PV Metrology Lab of NIM (National Institute of Metrology, China). Measurement of irradiance intensity and all other measurements are traceable to the International System of Units (SI). Data in this report apply only at the time of the test for the sample. For more details, please refer to the text of the report.

	Area (mm²)	I_{sc}(mA)	V_{oc}(V)	P_{max}(mW)
Reverse Scan	10.128	2.384	1.158	2.274
Forward Scan	10.128	2.366	1.155	2.212
	I_{max}(mA)	V_{max}(V)	FF (%)	η (%)
Reverse Scan	2.251	1.010	82.3	22.5
Forward Scan	2.234	0.990	81.0	21.8

I-V Characterization Methods:
JJF 1622-2017: Calibration Specification of Solar Cells：Photoelectric Properties
Reference Solar Cell:
Type: Mono-Si
Solar Simulator:
Classification: AAA (Double-light source: Xeon and Halogen);
Total irradiance: 1000 W/m² based on I_{sc} of the above Reference Solar Cell.

Report No.: GXgf2022-00881
DUT S/N：Flex 10-M2

I-V Characteristic curves and parameters (Reverse & Forward Scan)

Steady-state scanning curve (V_{bias} = 1.010 V, $t_{scanning}$ = 300 s, P_{start}= 2.185 mW and P_{finish}= 2.211 mW)

Figure S13. Certification results of flexible perovskite solar cells by the National Institute of Metrology, China (NIM, China).

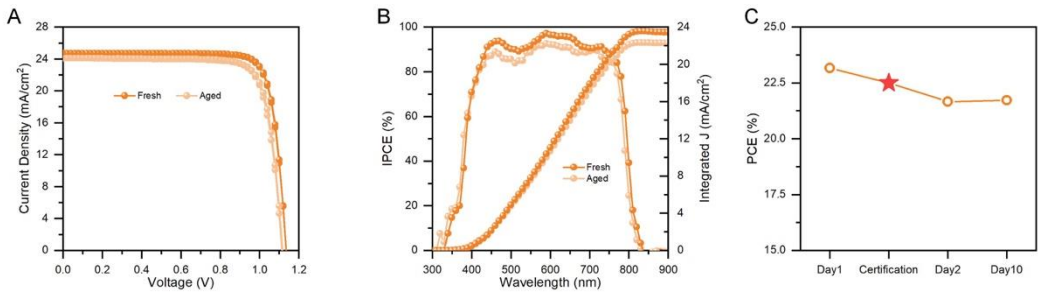

Figure S14. Performance of the unencapsulated fresh and aged MS-FPSC before and after certification. (A) *J-V* curves and (B) IPCE spectra of the unencapsulated fresh and aged flexible device. (C) PCE change of the certified MS-FPSC before and after certification. The day before certification is designated as Day 1. The take-out process led to a decline in the device performance, which can also be revealed in the current density, while it maintained the efficiency after storage in the dry box in our lab.

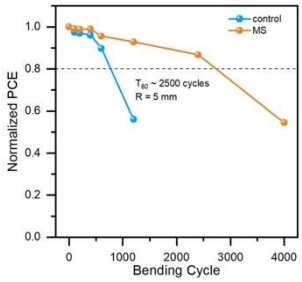

Figure S15. Normalized PCEs of control and MS-FPSCs after different bending cycles (bending radius = 5 mm, ~30% RH, ~ 25 °C).

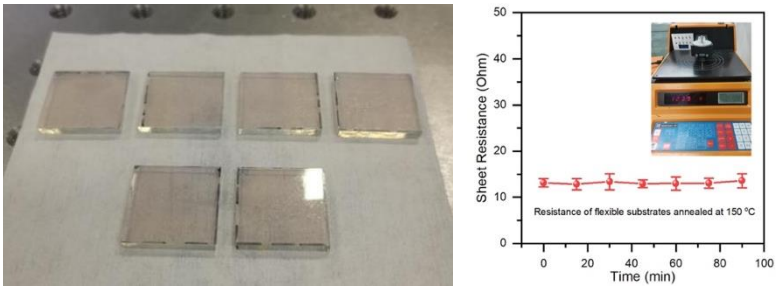

Figure S16. Images of flexible substrates after thermal annealing at 150 °C and the sheet resistance recorded during the annealing process. Carefully attached flexible substrates showed no deformation after the annealing process, and the sheet resistance remained normal.

Table S3. Extracted diffraction angle and FWHM data in Figure 3C, 3D.

Sample	2θ/°	FWHM/°	θ/rad	FWHM/rad	$4\sin\theta$	$\beta_T \cos\theta$
control	13.959	0.145	0.12182	0.00253	0.48606	0.00251
	19.82	0.164	0.17296	0.00286	0.6884	0.00282
	24.339	0.166	0.2124	0.0029	0.84322	0.00283
	28.121	0.149	0.2454	0.0026	0.97179	0.00252
	31.56	0.16	0.27541	0.00279	1.08778	0.00269
	40.281	0.204	0.35152	0.00356	1.37729	0.00334
	42.82	0.247	0.37367	0.00431	1.46016	0.00401
MS	13.999	0.142	0.12216	0.00248	0.48744	0.00246
	19.84	0.169	0.17314	0.00295	0.68909	0.00291
	24.36	0.146	0.21258	0.00255	0.84393	0.00249
	28.162	0.149	0.24576	0.0026	0.97317	0.00252
	31.581	0.15	0.2756	0.00262	1.08848	0.00252
	40.281	0.161	0.35152	0.00281	1.37729	0.00264
	42.84	0.2	0.37385	0.00349	1.46081	0.00325

Table S4. Extracted diffraction angle and FWHM data in Figure S9.

Sample	2θ/°	FWHM/°	θ/rad	FWHM/rad	$4\sin\theta$	$\beta_T \cos\theta$
control	14.06	0.153	0.1227	0.00267	0.48956	0.00265
	19.917	0.127	0.17381	0.00222	0.69174	0.00218
	24.4	0.187	0.21293	0.00326	0.8453	0.00319
	31.659	0.15	0.27628	0.00262	1.0911	0.00252
	34.781	0.276	0.30352	0.00482	1.19553	0.0046
MS	14.018	0.144	0.12233	0.00251	0.4881	0.00249
	19.861	0.1	0.17332	0.00175	0.68981	0.00172
	24.344	0.172	0.21244	0.003	0.84339	0.00293
	31.636	0.159	0.27608	0.00278	1.09033	0.00267
	34.701	0.158	0.30282	0.00276	1.19287	0.00263

Table S5. FWHM and estimated crystalline sizes of control and MS-perovskite films.

Sample	FWHM at (100)/°	Estimated Crystalline Sizes (nm)
control	0.145	55.2
MS	0.142	56.3

Table S6. Absorption energy of succinate anions on the $FAPbI_3$ surface.

	E_{abs}	$E_{MS+FAPbI_3}$	E_{MS}	E_{FAPbI_3}
FAI-terminated	-4.86	-2543.11	-73.64	-2464.62
PbI_2-terminated	-4.16	-2190.96	-73.61	-2113.19

References

1. Kaltenbrunner, M., Adam, G., Glowacki, E.D., et al. (2015). Flexible high power-per-weight perovskite solar cells with chromium oxide-metal contacts for improved stability in air. Nat Mater ***14***, 1032-1039.

2. Bu, T., Li, J., Li, H., et al. (2021). Lead halide-templated crystallization of methylamine-free perovskite for efficient photovoltaic modules. Science ***372***, 1327-1332.

3. Li, M., Zhou, J., Tan, L., et al. (2022). Brominated PEAI as multi-functional passivator for high-efficiency perovskite solar cell. Energy & Environ. Mater. eem2.12360.

4. Kresse, G., and Joubert, D. (1999). From ultrasoft pseudopotentials to the projector augmented-wave method. Phys. Rev. B ***59***, 1758-1775.

5. Perdew, J.P., Burke, K., and Ernzerhof, M. (1996). Generalized gradient approximation made simple. Phys. Rev. Lett. ***77***, 3865-3868.

6. Blöchl, P.E. (1994). Projector augmented-wave method. Phys. Rev. B ***50***, 17953-17979.

7. Grimme, S., Antony, J., Ehrlich, S., and Krieg, H. (2010). A consistent and accurate ab initio parametrization of density functional dispersion correction (DFT-D) for the 94 elements H-Pu. J. Chem. Phys. ***132***, 154104.